Nonequilibrium Dynamics of Dirac Quantum Criticality in Imaginary Time

Yin-Kai Yu,[1,2,3,4] Zhi Zeng,[1,2] Yu-Rong Shu,[5] Zi-Xiang Li,[3,4,*] and Shuai Yin[1,2,†]
[1]Guangdong Provincial Key Laboratory of Magnetoelectric Physics and Devices, Sun Yat-Sen University, Guangzhou 510275, China
[2]School of physics, Sun Yat-Sen University, Guangzhou 510275, China
[3]Beijing National Laboratory for Condensed Matter Physics and Institute of Physics, Chinese Academy of Sciences, Beijing 100190, China
[4]University of Chinese Academy of Sciences, Beijing 100049, China
[5]School of Physics and Materials Science, Guangzhou University, Guangzhou 510006, China

(Received 21 December 2023; revised 22 October 2025; accepted 4 February 2026; published 24 February 2026)

Quantum criticality within Dirac fermions harbors a plethora of exotic phenomena, attracting sustained attention in the past decades. Here, we explore the imaginary-time relaxation dynamics in a typical Dirac quantum criticality belonging to chiral Heisenberg universality class. Performing large-scale quantum Monte Carlo simulation, we unveil rich nonequilibrium critical phenomena from different initial states. In particular, we identify a nonstationary initial slip evolution characterized by an unconventional negative critical exponent $\theta = -0.84(4)$, corroborating the significant impact of fermionic critical fluctuations. Furthermore, we generalize the nonequilibrium scaling theory to incorporate both fermionic and bosonic critical modes, capturing their distinct relaxation behaviors. Armed with the scaling theory, we establish a new framework to investigate fermionic quantum criticality based on short-time dynamics, paving a promising avenue to fathoming quantum criticality in diverse fermionic systems with high efficiency.

DOI: 10.1103/7ltm-f68w

Introduction—Quantum phase transitions, describing abrupt changes in ground states of quantum systems, are central topics in modern physics [1]. A prominent example is the interaction-driven quantum criticality in Dirac systems. Such transitions were originally discussed in high-energy physics to mimic chiral symmetry breaking and spontaneous mass generation [2]. Recently, owing to the inspiring experimental advances in graphene [3] and topological materials [4,5], quantum criticality in Dirac fermions has garnered increasing interest in condensed matter physics. Vast efforts have been made in this field, including sophisticated renormalization group analyses [6–17], conformal bootstrap [18], quantum Monte Carlo simulation [19–33], and the tensor network method [34,35], resulting in tremendous achievements. It has been shown that fluctuations from gapless Dirac fermions enormously fertilize the fundamental research of quantum criticality, not only contributing to the Gross-Neveu fixed point [6–52], which is among the simplest examples of quantum critical points that do not exhibit classical analogs, but also yielding a profound mechanism for the Landau-forbidden quantum criticality [53–59].

On the other hand, universal critical phenomena are manifested not only in the long-time equilibrium states but also in short-time nonequilibrium processes [60–64]. For instance, in classical systems, the relaxation dynamics shows a nonstationary initial slip evolution in the short-time stage, and an additional critical initial slip exponent, which is usually positive, is required to describe this phenomenon [65–67]. Similar short-time scaling behaviors also arise in real-time critical dynamics in quantum systems [68–75]. In particular, in Dirac systems, the field theory predicted that fluctuations from the Dirac fermions can induce a negative critical initial slip exponent [73].

Aside from the real-time dynamics, imaginary-time dynamics in quantum systems is also of great interest and significance. As a routine unbiased approach to identifying the ground state, the imaginary-time evolution works extensively in numerical simulations, such as quantum Monte Carlo (QMC) and tensor networks. Near a quantum critical point (QCP), it was shown that the imaginary-time critical dynamics (ITCD) demonstrates colorful universal scaling behaviors [76–79]. So far, the ITCD has been studied in various quantum systems, providing an abundance of intriguing perspectives in the field of quantum criticality [79–86].

Moreover, the imaginary-time dynamics also finds its practical applications in fast-developing quantum programmable devices including quantum circuits simulating fermionic systems [87–89], partly spurred by the recent availability of noisy intermediate-scale quantum hardware and Rydberg atomic systems, to explore various exotic

*Contact author: zixiangli@iphy.ac.cn
†Contact author: yinsh6@mail.sysu.edu.cn

 © 2026 American Physical Society

quantum phases [90–93]. As a win-win case, these quantum devices also provide platforms to experimentally realize ITCD and demonstrate its power in determining the critical properties with high efficiency and scalability, circumventing difficulties induced by critical slowing down and divergent entanglement in conventional methods based on equilibrium scaling [94].

However, nonequilibrium dynamics in Dirac quantum criticality remains largely unexplored. This kind of quantum criticality is fundamentally different from the previously studied paradigms of ITCD [79], which feature a single type of critical fluctuation such as bosonic order parameters. The key difference lies in the coexistence of fermionic and bosonic critical fluctuations in the Dirac criticality. Given the many intriguing features of gapless Dirac fermions in equilibrium, how these fluctuations influence nonequilibrium dynamics is a compelling question.

Following this line of inquiry, we investigate the ITCD of a paradigmatic Dirac-fermion QCP, namely the chiral Heisenberg Gross-Neveu transition hosted by the honeycomb Hubbard model [36–40]. Employing sign-problem-free QMC simulations [95–103], we find that the system exhibits rich dynamic scaling behaviors for different initial states. We generalize the nonequilibrium scaling theory by unifying the scaling of both fermionic and bosonic correlations. In particular, we numerically find a negative critical initial slip exponent arising in the ITCD, in stark contrast to the bosonic systems, where the exponent is typically positive. We discuss the physical connection between this anomalous behavior and the gapless Dirac fermion fluctuations, corroborating that the dynamical feature of fermions in a real-time case [73] persists in imaginary-time dynamics. Moreover, our scaling theory allows for precise determination of the critical exponents of the chiral Heisenberg Gross-Neveu transition, in agreement with previous equilibrium studies, but using only short-time data. The proposed framework not only provides a unified understanding of nonequilibrium ITCD in Dirac systems but also offers a practical and general route for investigating critical properties in strongly correlated systems, even enabling the efficient preemption of the sign problem in fermionic QMC simulations [104].

Hamiltonian and dynamical protocol—To explore the dynamic scaling in the chiral Heisenberg universality class, we start with the Hubbard model defined on the honeycomb lattice, characterized by the Hamiltonian [36–40],

$$H = -t\sum_{\langle ij\rangle,\sigma} c_{i\sigma}^{\dagger} c_{j\sigma} + U\sum_{i}\left(n_{i\uparrow}-\frac{1}{2}\right)\left(n_{i\downarrow}-\frac{1}{2}\right), \quad (1)$$

where $c_{i\sigma}^{\dagger}$ ($c_{j\sigma}$) represents the creation (annihilation) operator of electrons with spin polarization σ, $n_{i\sigma} \equiv c_{i\sigma}^{\dagger} c_{i\sigma}$ is the electron number operator, t is the hopping amplitude between the nearest neighbor sites, and U represents the strength of on-site repulsive interaction. As shown in Fig. 1, when $U/t \ll 1$ the system is in the Dirac semimetal (DSM) phase characterized by the four-component Dirac excitation with flavor number $N_f = 2$, whereas for large $U/t \gg 1$ the system hosts an antiferromagnetic (AFM) phase with a finite charge gap. A phase transition separating these two phases happens at a finite $U_c/t \approx 3.9$ and belongs to the chiral Heisenberg universality class [36–40]. For simplicity, we set t to unity in subsequent discussions.

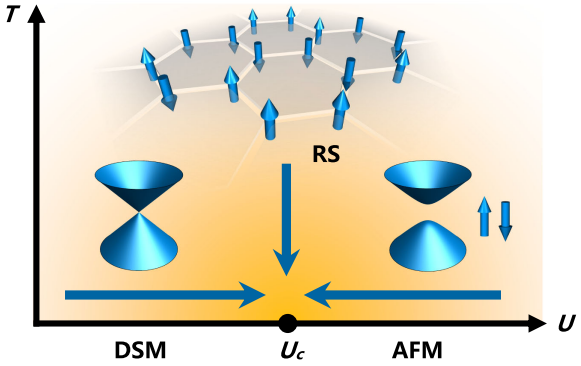

FIG. 1. Phase diagram and the quench protocol in imaginary time with different initial states. The initial states are prepared as (i) the Dirac semimetal (DSM) phase, (ii) the saturated AFM state, and (iii) the random spin (RS) state. All states correspond to the fixed points of the initial states under the renormalization group transformation.

For the imaginary-time relaxation dynamics, the wave function $|\psi(\tau)\rangle$ evolves according to the imaginary-time Schrödinger equation $-(\partial/\partial\tau)|\psi(\tau)\rangle = H|\psi(\tau)\rangle$ imposed by the normalization condition. The formal solution of the Schrödinger equation is given by $|\psi(\tau)\rangle = e^{-\tau H}|\psi(0)\rangle/Z(\tau)$, where $Z(\tau) \equiv \langle\psi(\tau)|\psi(\tau)\rangle$ is the normalization factor and $|\psi(0)\rangle$ is the initial wave function. As illustrated in Fig. 1, we consider three kinds of initial states: (i) the saturated AFM state, (ii) the noninteracting DSM state, and (iii) the random spin (RS) state. In the following, we employ the large-scale determinant QMC method to simulate the ITCD.

General scaling theory—Generally, for an observable P its dynamic scaling in ITCD should satisfy [79,105]

$$P(\tau, g, L, \{X\}) = \tau^{-\frac{\kappa}{z}} f_P\left(g\tau^{\frac{1}{\nu z}}, L^{-1}\tau^{\frac{1}{z}}, \{X\tau^{-\frac{c}{z}}\}\right), \quad (2)$$

where $g \equiv (U - U_c)$, L is the lattice size, κ is the scaling dimension of P, ν is the correlation length exponent, z is the dynamic exponent, and $z = 1$ for the Dirac QCP in Eq. (1) [This value can be determined via ITCD as discussed in Supplemental Material (SM) [106]]. $\{X\}$ with its exponent c represents the possible relevant variables associated with the initial state.

Three remarks on Eq. (2) are listed as follows. (1) For $\tau \to \infty$, Eq. (2) recovers the usual finite-size scaling and $\{X\}$ becomes irrelevant. (2) All three kinds of initial states

studied here, namely AFM, DSM, and RS, correspond to three fixed points, respectively [114]. Thus, $\{X\}$ does not explicitly appear in Eq. (2). However, scaling functions f_P vary for different initial states. (3) We mainly focus on the short-time scale $1 \ll \tau \ll L^z$ in the sense of a field theory. This is distinct from both the long-time scale $\tau \gg L^z$ required for reaching the ground state and the microscopic ultraviolet time scale. In this window, the system enters a nonequilibrium universal scaling regime governed by the underlying QCP.

Relaxation dynamics with the AFM initial state—First, we study the ITCD starting with the AFM initial state. To illustrate the nonequilibrium scaling properties, we explore the dynamics of the correlation-length ratio defined as $R \equiv S(\mathbf{0})/S(\Delta\boldsymbol{q})$ [115], where $\Delta\boldsymbol{q}$ is minimum lattice momentum and $S(\boldsymbol{q})$ is the antiferromagnetic structure factor $S(\boldsymbol{q}) = (1/L^{2d})\sum_{i,j} e^{i\boldsymbol{q}\cdot(\boldsymbol{r}_i-\boldsymbol{r}_j)}\langle S_i^z S_j^z\rangle$ with S_i^z being the staggered magnetization operator defined as $S_i^z \equiv \frac{1}{2}\boldsymbol{c}_{i,A}^\dagger\sigma^z\boldsymbol{c}_{i,A} - \frac{1}{2}\boldsymbol{c}_{i,B}^\dagger\sigma^z\boldsymbol{c}_{i,B}$ and $\boldsymbol{c}^\dagger \equiv (c_\uparrow^\dagger, c_\downarrow^\dagger)$.

As a dimensionless variable, R in the ITCD obeys the following dynamic scaling form according to Eq. (2):

$$R(g,\tau,L) = f_R(gL^{1/\nu}, \tau L^{-z}), \tag{3}$$

which indicates that, with a fixed τL^{-z}, R does not depend on the system size when $g = 0$, thereby providing a method to pinpoint the critical point.

As shown in Fig. 2(a), we calculate R as a function of U with fixed $\tau L^{-z} = 0.3$ for different sizes and find that the curves almost cross at a point. Accordingly, we determine the critical point as $U_c = 3.91(3)$ [see details in SM [106]]. Upon fixing $U_c = 3.91$ into Eq. (3), we adjust the value of ν for the rescaled horizontal variable $gL^{1/\nu}$ to make curves of different sizes collapse, yielding the value of ν as $\nu = 1.17(7)$. Both values of U_c and ν are consistent with those obtained from equilibrium method, albeit slight deviations arise possibly due to the scaling corrections [8,40]. Remarkably, significantly less effort is required as the results are obtained in the short-time stage, and long enough imaginary-time evolution to achieve the ground state in the usual equilibrium method is not required here. Moreover, Eq. (3) also provides a self-consistent way to confirm the results. As shown in Fig. 2 and SM [106], for different τL^{-z}, consistent U_c and ν are obtained in a similar way, highlighting the validity of Eq. (3).

To delve deeper into the ITCD of model (1), we study scaling behaviors of the square of order parameter $m^2 = S(0)$. In the following, we focus on the case with $g = 0$. The off-critical-point effects are discussed in SM [106]. According to Eq. (2), for the saturated AFM initial state, m^2 should satisfy [66,79]

$$m^2(\tau,L) = \tau^{-2\beta/\nu z} f_m(\tau L^{-z}), \tag{4}$$

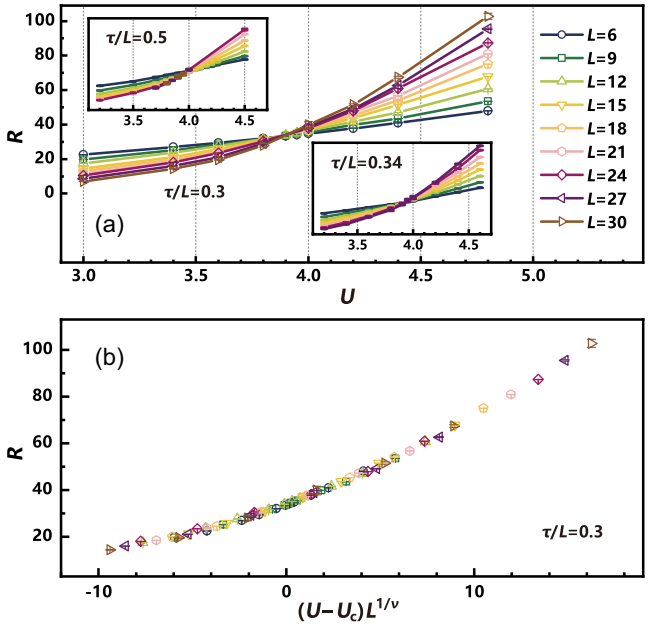

FIG. 2. Results of correlation-length ratio R against interaction U for various sizes during the short-time stage, with a fixed value of τL^{-z}. (a) Estimation of the critical point via the intersection points of curves for $\tau L^{-z} = 0.3$ (main panel) 0.34 and 0.5 (inset). (b) Estimation of ν by scaling collapse analysis of the correlation-length ratio.

where β/ν is the scaling dimension of m. Note that Eq. (4) can be transformed to $m^2(\tau,L) = L^{-2\beta/\nu} f_{m1}(\tau L^{-z})$ [116] so that the usual finite-size scaling is recovered as $\tau \to \infty$.

Figure 3(a1) shows the evolution of m^2 for different L. At first, as shown in Fig. 3(a2), data collapse analysis of the results yields the exponent $\beta/\nu = 0.80(3)$, which is close to the result obtained via equilibrium methods [39,40]. The collapse of rescaled results for different L into a single curve unequivocally demonstrates the dynamic scaling behavior with AFM as the initial state, as depicted in Eq. (4). Moreover, as shown in Fig. 3(a1), one finds that, in the short-time stage, $m^2 \propto \tau^{-2\beta/\nu z}$ and the scaling behavior is almost independent of the system size. The underlying reason is that the initial state is an uncorrelated state and the correlation length ξ increases with time as $\xi \propto \tau^{1/z}$. In the short-time stage, $\xi < L$ and the finite-size effects are negligible, whereas in the long-time stage, $\xi > L$ and the system enters the finite-size scaling region in which $m^2 \propto L^{-2\beta/\nu}$. These results demonstrate that it is feasible to infer critical properties in the thermodynamic limit directly from the short-time dynamics.

Then we turn to the ITCD of the fermion correlation defined as $G(\Delta\boldsymbol{q}) \equiv (1/L^d)\sum_{ij} e^{i(K+\Delta\boldsymbol{q})\cdot(\boldsymbol{r}_i-\boldsymbol{r}_j)} c_{i,A}^\dagger c_{j,B}$, with K being the momentum at the Dirac point. According to Eq. (2), the scaling form of G should be

$$G(\tau,L) = \tau^{-\eta_\psi/z} f_G(\tau L^{-z}), \tag{5}$$

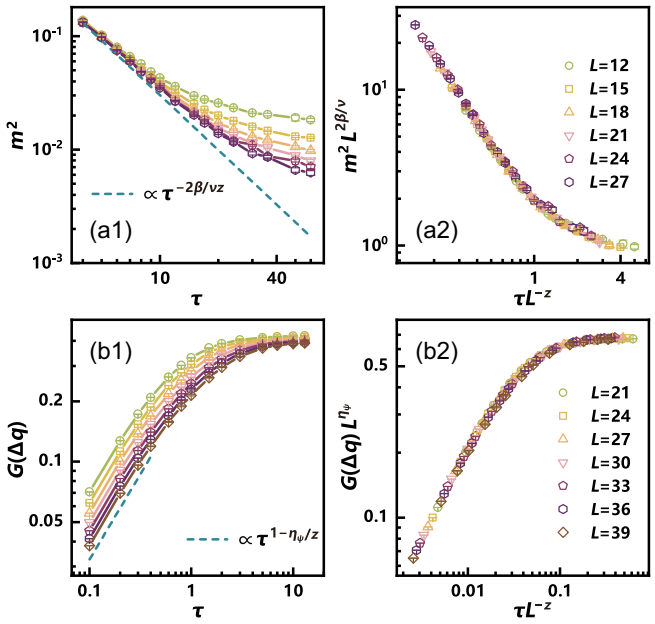

FIG. 3. Relaxation dynamics at QCP with the AFM initial state. (a) Curves of m^2 versus τ for different sizes before (a1) and after (a2) rescaling. The dashed line in (a1) representing $m^2 \propto \tau^{-2\beta/\nu z}$ with β/ν estimated from (a2) is plotted for comparison. (b) Curves of G versus τ before (b1) and after (b2) rescaling. The dashed line in (b1) represents $G \propto \tau^{1-\eta_\psi/z}$ with η_ψ estimated from (b2).

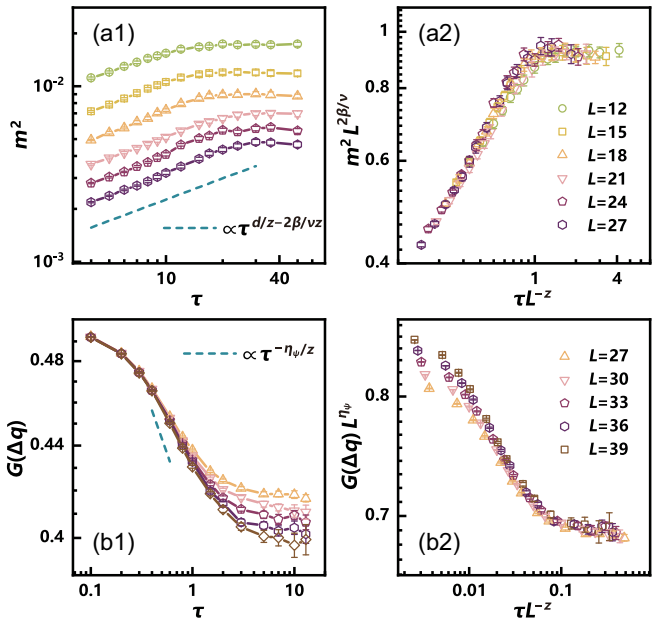

FIG. 4. Relaxation dynamics at QCP with the DSM initial state. (a) Curves of m^2 versus τ at the critical point for different sizes before (a1) and after (a2) rescaling. The dashed line representing $m^2 \propto \tau^{d/z-2\beta/\nu z}$ is plotted in (a1) for comparison. (b) Curves of G versus τ before (b1) and after (b2) rescaling. The dashed line in (b1) represents $G \propto \tau^{-\eta_\psi/z}$. The critical exponents used here are estimated from Fig. 3.

where η_ψ is the anomalous dimension of the fermion operator. It was shown that G is closely related to the quasiparticle weight Z [106], whose singularity was observed in the fermionic criticality [117], and also scales with η_ψ [106]. Moreover, the fact that $G = 0$ at the saturated AFM initial state dictates the absence of the constant term in the short-time expansion of $f_G(\tau L^{-z})$. Thus, Eq. (5) can be transformed into

$$G(\tau, L) = \tau^{1-\eta_\psi/z} L^{-z} f_{G1}(\tau L^{-z}). \tag{6}$$

Figure 3(b1) shows the evolution of G at $g = 0$ for different L. Data collapse analysis in Fig. 3(b2) gives $\eta_\psi = 0.15(4)$, which is close to the result obtained via equilibrium methods [40,107]. Moreover, Fig. 3(b1) shows that, in the short-time stage, $G \propto \tau^{1-\eta_\psi/z}$. These results not only confirm Eq. (6) but also demonstrate that the critical exponent for fermion correlation can be determined from the ITCD.

Relaxation dynamics with the DSM initial state—We proceed to explore the ITCD from the noninteracting DSM state. For this state, it is straightforward to show that $m^2 \propto L^{-d}$. This size-dependent scaling affects the relaxation dynamics in the short-time stage, giving rise to the dynamic scaling of m^2:

$$m^2(\tau, L) = L^{-d} \tau^{d/z-2\beta/\nu z} f_{m2}(\tau L^{-z}). \tag{7}$$

To demonstrate the dynamic scaling Eq. (7), we show in Fig. 4(a) the evolution of m^2 at $g = 0$. In the short-time stage, m^2 increases as $m^2 \propto \tau^{d/z-2\beta/\nu z}$ for given L, qualitatively different from the dynamic behavior with AFM initial state. In addition, by rescaling m^2, and τ according to Eq. (2) with the exponents determined in previous section, one finds that the curves collapse onto each other. These results reveal the dynamic scaling behavior with the DSM initial state described by Eq. (7).

We also study the dynamics of fermion correlation G as shown in Fig. 4(b). In the short-time stage, Fig. 4(b1) shows that G tends toward the curve of $G \propto \tau^{-\eta_\psi/z}$ as L increases. Moreover, the scaling collapse in Fig. 4(b2) with exponents determined in the previous section confirms Eq. (5).

Critical initial slip with the RS initial state—Then we study the ITCD from the RS state, for which every site has one electron with its spin randomly distributed. With this uncorrelated initial state, the evolution of m^2 and G satisfy Eq. (7) except for a different scaling function, as discussed in SM [106].

Furthermore, when initiating from the RS state, we observe a universal critical initial slip behavior in the short-time stage [65,66,79]. Intriguingly, the scaling property of the initial slip behavior is determined by an independent dynamic exponent θ, which does not exist in the equilibrium critical behavior. To characterize the critical initial slip, the autocorrelation function A was

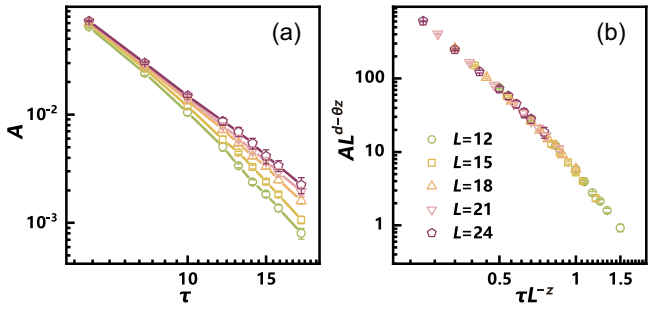

FIG. 5. Critical initial slip manifested in the evolution of the autocorrelation function A with the RS initial state. Curves of A versus τ for different sizes at the critical point before (a) and after (b) rescaling.

introduced, defined as $A = (1/L^d)\sum_i \overline{\langle S_i(0)\rangle \langle S_i(\tau)\rangle}$ [108], where the overline denotes the average on the initial state configurations. At the critical point, A obeys the following scaling form [108]:

$$A(\tau) = \tau^{-d/z+\theta} f_A(\tau L^{-z}). \tag{8}$$

As shown in Fig. 5, by rescaling A and τ according to Eq. (8) and adjusting the trial value of the θ to make the rescaled curves collapse onto each other, we access the dynamic exponent $\theta = -0.84(4)$.

The negative exponent θ is notably interesting since it is in sharp contrast to classical criticality, where θ is typically positive. To illustrate the underlying physics, it is intuitive to consider the short-time dynamics of m from an initial RS state with a small residual magnetization m_0. It was shown that m evolves as $m \propto m_0 \tau^\theta$ in the short-time stage [65], governed by the competition between domain growth and critical fluctuations. In classical systems, critical fluctuations of the order parameter are not yet developed at early times, allowing magnetic domains to grow around the m_0 seeds and yielding $\theta > 0$. This scenario also holds for the quantum Ising model [79,106], where bosonic order-parameter correlations remain weak in the short-time stage and the $\theta > 0$ critical initial slip originates from the mean-field tendency toward ordering [79]. By contrast, in Dirac criticality, fermion correlations rapidly build up and equilibrate much earlier than their bosonic counterparts (see SM [106], Fig. S4). This may arise from the linear dispersion and low density of states near the Dirac point, which lead to higher characteristic energies and shorter relaxation times than those of the bosonic modes. Consequently, the imaginary-short-time dynamics of the system is dominated by critical fluctuations of gapless fermions, while magnetic ordering is suppressed, resulting in a negative critical initial slip exponent $\theta < 0$, in analogy to the real-time case [73].

Discussions and concluding remarks—In summary, we perform sign-problem-free QMC simulations to investigate the ITCD in a Dirac QCP belonging to the chiral Heisenberg universality class. For the first time, we extend the nonequilibrium scaling theory to Dirac systems and establish the corresponding scaling forms for different initial states, thereby revealing rich nonequilibrium dynamic scaling behaviors. In particular, a negative critical initial slip exponent $\theta = -0.84(4)$ is observed in the ITCD from the RS initial state, remarkably different from the classical cases in which θ is usually positive, confirming the role of fermion fluctuations in relaxation dynamics [73].

Our Letter also paves a new way to decipher the critical properties of quantum phase transitions in fermionic systems. Compared with the usual methods tackling critical properties in the equilibrium ground state, the nonequilibrium method is highly efficient, since critical exponents are accessed by the short imaginary-time evolution. More crucially, our Letter offers a possible route to studying fermionic QCP in the presence of sign problem, which is the main obstacle hindering the understanding of QCP by numerical approaches. Since the severity of sign problem exponentially increases with imaginary time in the process of evolution, the simulation on relatively large system sizes usually remains accessible in the stage of short imaginary time. Hence, it is promising to access the quantum critical behavior even when the model under consideration is sign problematic [104].

Moreover, inspired by the experimental realization of the ITCD in a quantum computer platform [94] and remarkable progresses made in fermionic quantum processors [92,93], it is expected that our present Letter can be experimentally realized and contribute an efficient approach to detecting quantum criticality in these quantum devices in the near future. In addition, it was shown that the driven critical dynamics and the shallow sudden quench critical dynamics are all described by the equilibrium critical exponents [61,62,73,118,119]. Accordingly, the critical exponents determined here are also applicable to these kinds of dynamics in Dirac criticality [118].

Acknowledgments—Y.-K. Y., Z. Z., and S. Y. are supported by the National Natural Science Foundation of China under Grants No. 12222515 and No. 12075324, the Research Center for Magnetoelectric Physics of Guangdong Province under Grant No. 2024B0303390001, and the Guangdong Provincial Key Laboratory of Magnetoelectric Physics and Devices under Grant No. 2022B1212010008. S. Y. is also supported by the Science and Technology Projects in Guangdong Province under Grant No. 2021QN02X561 and Guangzhou City under Grant No. 2025A04J5408. Z.-X. L. is supported by the start-up grant of IOP-CAS, the National Natural Science Foundation of China under Grants No. 12347107 and No. 12474146, the Beijing Natural Science Foundation under Grant No. JR25007, and the New Cornerstone Investigator Program. Y.-R. S. is supported by the

National Natural Science Foundation of China under Grant No. 12104109. Y.-K. Y. and Z. Z. are also supported by the (national) college students innovation and entrepreneurship training program, Sun Yat-sen University.

Data availability—The data that support the findings of this article are openly available [120].

[1] S. Sachdev, *Quantum Phase Transitions*, 2nd ed. (Cambridge University Press, Cambridge, England, 2011).
[2] D. J. Gross and A. Neveu, Phys. Rev. D **10**, 3235 (1974).
[3] A. H. Castro Neto, F. Guinea, N. M. R. Peres, K. S. Novoselov, and A. K. Geim, Rev. Mod. Phys. **81**, 109 (2009).
[4] M. Z. Hasan and C. L. Kane, Rev. Mod. Phys. **82**, 3045 (2010).
[5] X.-L. Qi and S.-C. Zhang, Rev. Mod. Phys. **83**, 1057 (2011).
[6] L. N. Mihaila, N. Zerf, B. Ihrig, I. F. Herbut, and M. M. Scherer, Phys. Rev. B **96**, 165133 (2017).
[7] N. Zerf, L. N. Mihaila, P. Marquard, I. F. Herbut, and M. M. Scherer, Phys. Rev. D **96**, 096010 (2017).
[8] K. Ladovrechis, S. Ray, T. Meng, and L. Janssen, Phys. Rev. B **107**, 035151 (2023).
[9] L. Janssen and I. F. Herbut, Phys. Rev. B **89**, 205403 (2014).
[10] B. Knorr, Phys. Rev. B **94**, 245102 (2016).
[11] J. A. Gracey, T. Luthe, and Y. Schröder, Phys. Rev. D **94**, 125028 (2016).
[12] B. Roy, V. Juričić, and I. F. Herbut, J. High Energy Phys. 04 (2016) 018.
[13] F. Gehring, H. Gies, and L. Janssen, Phys. Rev. D **92**, 085046 (2015).
[14] B. Ihrig, L. N. Mihaila, and M. M. Scherer, Phys. Rev. B **98**, 125109 (2018).
[15] R. Boyack, H. Yerzhakov, and J. Maciejko, Eur. Phys. J. Special Topics **230**, 979 (2021).
[16] B. Roy and S. Das Sarma, Phys. Rev. B **94**, 115137 (2016).
[17] S. Han, G. Y. Cho, and E.-G. Moon, Phys. Rev. B **98**, 085149 (2018).
[18] D. Poland, S. Rychkov, and A. Vichi, Rev. Mod. Phys. **91**, 015002 (2019).
[19] T. C. Lang and A. M. Läuchli, Phys. Rev. Lett. **123**, 137602 (2019).
[20] Z. H. Liu, W. Jiang, B.-B. Chen, J. Rong, M. Cheng, K. Sun, Z. Y. Meng, and F. F. Assaad, Phys. Rev. Lett. **130**, 266501 (2023).
[21] Z.-X. Li, A. Vaezi, C. B. Mendl, and H. Yao, Sci. Adv. **4**, eaau1463 (2018).
[22] S. Gazit, M. Randeria, and A. Vishwanath, Nat. Phys. **13**, 484 (2017).
[23] Z. Zhou, D. Wang, Z. Y. Meng, Y. Wang, and C. Wu, Phys. Rev. B **93**, 245157 (2016).
[24] S. M. Tabatabaei, A.-R. Negari, J. Maciejko, and A. Vaezi, Phys. Rev. Lett. **128**, 225701 (2022).
[25] Y. Otsuka, K. Seki, S. Sorella, and S. Yunoki, Phys. Rev. B **98**, 035126 (2018).
[26] X. Y. Xu and T. Grover, Phys. Rev. Lett. **126**, 217002 (2021).
[27] Y. Liu, W. Wang, K. Sun, and Z. Y. Meng, Phys. Rev. B **101**, 064308 (2020).
[28] S. Chandrasekharan and A. Li, Phys. Rev. D **88**, 021701 (2013).
[29] X. Zhu, Y. Huang, H. Guo, and S. Feng, Phys. Rev. B **106**, 075109 (2022).
[30] T.-T. Wang and Z. Y. Meng, Phys. Rev. B **108**, L121112 (2023).
[31] H. Xu, X. Li, Z. Zhou, X. Wang, L. Wang, C. Wu, and Y. Wang, Phys. Rev. Res. **5**, 023180 (2023).
[32] X.-J. Yu, Z. Pan, L. Xu, and Z.-X. Li, Phys. Rev. Lett. **132**, 116503 (2024).
[33] X.-J. Yu, S.-H. Shi, L. Xu, and Z.-X. Li, Phys. Rev. Lett. **132**, 036704 (2024).
[34] P. Corboz, P. Czarnik, G. Kapteijns, and L. Tagliacozzo, Phys. Rev. X **8**, 031031 (2018).
[35] M. Rader and A. M. Läuchli, Phys. Rev. X **8**, 031030 (2018).
[36] S. Sorella and E. Tosatti, Europhys. Lett. **19**, 699 (1992).
[37] I. F. Herbut, Phys. Rev. Lett. **97**, 146401 (2006).
[38] I. F. Herbut, V. Juričić, and O. Vafek, Phys. Rev. B **80**, 075432 (2009).
[39] F. F. Assaad and I. F. Herbut, Phys. Rev. X **3**, 031010 (2013).
[40] Y. Otsuka, S. Yunoki, and S. Sorella, Phys. Rev. X **6**, 011029 (2016).
[41] T. Grover, D. N. Sheng, and A. Vishwanath, Science **344**, 280 (2014).
[42] U. F. P. Seifert, X.-Y. Dong, S. Chulliparambil, M. Vojta, H.-H. Tu, and L. Janssen, Phys. Rev. Lett. **125**, 257202 (2020).
[43] S. Ray and L. Janssen, Phys. Rev. B **104**, 045101 (2021).
[44] Y. Da Liao, X. Y. Xu, Z. Y. Meng, and Y. Qi, Phys. Rev. B **106**, 075111 (2022).
[45] L. Wang, P. Corboz, and M. Troyer, New J. Phys. **16**, 103008 (2014).
[46] Z.-X. Li, Y.-F. Jiang, and H. Yao, New J. Phys. **17**, 085003 (2015).
[47] Y. Liu, Z. Wang, T. Sato, W. Guo, and F. F. Assaad, Phys. Rev. B **104**, 035107 (2021).
[48] Z. H. Liu, M. Vojta, F. F. Assaad, and L. Janssen, Phys. Rev. Lett. **128**, 087201 (2022).
[49] C. Chen, X. Y. Xu, Z. Y. Meng, and M. Hohenadler, Phys. Rev. Lett. **122**, 077601 (2019).
[50] Y.-X. Zhang, W.-T. Chiu, N. C. Costa, G. G. Batrouni, and R. T. Scalettar, Phys. Rev. Lett. **122**, 077602 (2019).
[51] I. F. Herbut, Mod. Phys. Lett. B **38**, 2430006 (2024).
[52] Y. Otsuka, K. Seki, S. Sorella, and S. Yunoki, Phys. Rev. B **102**, 235105 (2020).
[53] Z.-X. Li, Y.-F. Jiang, S.-K. Jian, and H. Yao, Nat. Commun. **8**, 314 (2017).
[54] B.-H. Li, Z.-X. Li, and H. Yao, Phys. Rev. B **101**, 085105 (2020).
[55] E. Torres, L. Classen, I. F. Herbut, and M. M. Scherer, Phys. Rev. B **97**, 125137 (2018).
[56] L. Classen, I. F. Herbut, and M. M. Scherer, Phys. Rev. B **96**, 115132 (2017).
[57] Y.-Z. You, Y.-C. He, C. Xu, and A. Vishwanath, Phys. Rev. X **8**, 011026 (2018).

[58] S. Yin and Z.-Y. Zuo, Phys. Rev. B **101**, 155136 (2020).
[59] W. Hou and Y.-Z. You, Phys. Rev. B **108**, 125130 (2023).
[60] P. C. Hohenberg and B. I. Halperin, Rev. Mod. Phys. **49**, 435 (1977).
[61] J. Dziarmaga, Adv. Phys. **59**, 1063 (2010).
[62] A. Polkovnikov, K. Sengupta, A. Silva, and M. Vengalattore, Rev. Mod. Phys. **83**, 863 (2011).
[63] L. D'Alessio, Y. Kafri, A. Polkovnikov, and M. Rigol, Adv. Phys. **65**, 239 (2016).
[64] A. Mitra, Annu. Rev. Condens. Matter Phys. **9**, 245 (2018).
[65] H. K. Janssen, B. Schaub, and B. Schmittmann, Z. Phys. B **73**, 539 (1989).
[66] Z. B. Li, L. Schülke, and B. Zheng, Phys. Rev. Lett. **74**, 3396 (1995).
[67] E. V. Albano, M. A. Bab, G. Baglietto, R. A. Borzi, T. S. Grigera, E. S. Loscar, D. E. Rodriguez, M. L. R. Puzzo, and G. P. Saracco, Rep. Prog. Phys. **74**, 026501 (2011).
[68] E. G. Dalla Torre, E. Demler, and A. Polkovnikov, Phys. Rev. Lett. **110**, 090404 (2013).
[69] P. Gagel, P. P. Orth, and J. Schmalian, Phys. Rev. Lett. **113**, 220401 (2014).
[70] P. Gagel, P. P. Orth, and J. Schmalian, Phys. Rev. B **92**, 115121 (2015).
[71] A. Chiocchetta, M. Tavora, A. Gambassi, and A. Mitra, Phys. Rev. B **91**, 220302 (2015).
[72] A. Chiocchetta, A. Gambassi, S. Diehl, and J. Marino, Phys. Rev. Lett. **118**, 135701 (2017).
[73] S.-K. Jian, S. Yin, and B. Swingle, Phys. Rev. Lett. **123**, 170606 (2019).
[74] S. Yin and S.-K. Jian, Phys. Rev. B **103**, 125116 (2021).
[75] J. Marino, M. Eckstein, M. S. Foster, and A. M. Rey, Rep. Prog. Phys. **85**, 116001 (2022).
[76] C. De Grandi, A. Polkovnikov, and A. W. Sandvik, Phys. Rev. B **84**, 224303 (2011).
[77] C. De Grandi, A. Polkovnikov, and A. W. Sandvik, J. Phys. Condens. Matter **25**, 404216 (2013).
[78] C.-W. Liu, A. Polkovnikov, and A. W. Sandvik, Phys. Rev. B **87**, 174302 (2013).
[79] S. Yin, P. Mai, and F. Zhong, Phys. Rev. B **89**, 144115 (2014).
[80] Y.-R. Shu, S. Yin, and D.-X. Yao, Phys. Rev. B **96**, 094304 (2017).
[81] S. Zhang, S. Yin, and F. Zhong, Phys. Rev. E **90**, 042104 (2014).
[82] Y.-R. Shu, S.-K. Jian, and S. Yin, Phys. Rev. Lett. **128**, 020601 (2022).
[83] Y.-R. Shu and S. Yin, Phys. Rev. B **105**, 104420 (2022).
[84] Z. Zuo, S. Yin, X. Cao, and F. Zhong, Phys. Rev. B **104**, 214108 (2021).
[85] C.-W. Liu, A. Polkovnikov, and A. W. Sandvik, Phys. Rev. Lett. **114**, 147203 (2015).
[86] A. D. King *et al.*, Nature (London) **617**, 61 (2023).
[87] M. Motta, C. Sun, A. T. K. Tan, M. J. O'Rourke, E. Ye, A. J. Minnich, F. G. S. L. Brandão, and G. K.-L. Chan, Nat. Phys. **16**, 205 (2020).
[88] H. Nishi, T. Kosugi, and Y.-i. Matsushita, npj Quantum Inf. **7**, 85 (2021).
[89] S.-H. Lin, R. Dilip, A. G. Green, A. Smith, and F. Pollmann, PRX Quantum **2**, 010342 (2021).
[90] K. J. Satzinger *et al.*, Science **374**, 1237 (2021).
[91] G. Semeghini, H. Levine, A. Keesling, S. Ebadi, T. T. Wang, D. Bluvstein, R. Verresen, H. Pichler, M. Kalinowski, R. Samajdar, A. Omran, S. Sachdev, A. Vishwanath, M. Greiner, V. Vuleti, and M. D. Lukin, Science **374**, 1242 (2021).
[92] D. González-Cuadra, D. Bluvstein, M. Kalinowski, R. Kaubruegger, N. Maskara, P. Naldesi, T. V. Zache, A. M. Kaufman, M. D. Lukin, H. Pichler, B. Vermersch, J. Ye, and P. Zoller, Proc. Natl. Acad. Sci. U.S.A. **120**, e2304294120 (2023).
[93] T. V. Zache, D. González-Cuadra, and P. Zoller, Quantum **7**, 1140 (2023).
[94] S.-X. Zhang and S. Yin, Phys. Rev. B **109**, 134309 (2024).
[95] S. Sorella, S. Baroni, R. Car, and M. Parrinello, Europhys. Lett. **8**, 663 (1989).
[96] F. Assaad and H. Evertz, World-line and determinantal quantum Monte Carlo methods for spins, phonons and electrons, in *Computational Many-Particle Physics* (Springer, Berlin, Heidelberg, 2008), pp. 277–356.
[97] Z.-X. Li and H. Yao, Annu. Rev. Condens. Matter Phys. **10**, 337 (2019).
[98] M. Troyer and U.-J. Wiese, Phys. Rev. Lett. **94**, 170201 (2005).
[99] C. Wu and S.-C. Zhang, Phys. Rev. B **71**, 155115 (2005).
[100] Z.-X. Li, Y.-F. Jiang, and H. Yao, Phys. Rev. B **91**, 241117 (2015).
[101] Z.-X. Li, Y.-F. Jiang, and H. Yao, Phys. Rev. Lett. **117**, 267002 (2016).
[102] Z. C. Wei, C. Wu, Y. Li, S. Zhang, and T. Xiang, Phys. Rev. Lett. **116**, 250601 (2016).
[103] E. Berg, M. A. Metlitski, and S. Sachdev, Science **338**, 1606 (2012).
[104] Y.-K. Yu, Z.-X. Li, S. Yin, and Z.-X. Li, Sci. Adv. **12**, eadz4856 (2026).
[105] B. Zheng, Phys. Rev. Lett. **77**, 679 (1996).
[106] See Supplementary Material at http://link.aps.org/supplemental/10.1103/7ltm-f68w for detailed methodologies, additional analyses on the determination of the critical point, extended results on critical exponents, dynamic scaling from RS initial states, studies on critical initial slip, off-critical-point effects, and quasiparticle weight, which includes Refs. [9,19,24,40,65,79–81,96,105,107–113].
[107] K. Seki, Y. Otsuka, S. Yunoki, and S. Sorella, Phys. Rev. B **99**, 125145 (2019).
[108] B. Zheng, Int. J. Mod. Phys. B **12**, 1419 (1998).
[109] A. B. Migdal, Sov. Phys. JETP **5**, 333 (1957), https://www.jetp.ras.ru/cgi-bin/dn/e_005_02_0333.pdf.
[110] F. F. Assaad, M. Bercx, F. Goth, A. Götz, J. S. Hofmann, E. Huffman, Z. Liu, F. P. Toldin, J. S. E. Portela, and J. Schwab, SciPost Phys. Codebases 1 (2022).
[111] N. Hatano and M. Suzuki, Finding exponential product formulas of higher orders, in *Quantum Annealing and Other Optimization Methods*, edited by A. Das and B. K. Chakrabarti (Springer, Berlin, Heidelberg, 2005), pp. 37–68.
[112] F. F. Assaad, M. Imada, and D. J. Scalapino, Phys. Rev. B **56**, 15001 (1997).
[113] Y. Motome and M. Imada, J. Phys. Soc. Jpn. **66**, 1872 (1997).

[114] The random spin (RS) state remains invariant under coarse-graining or renormalization group transformations and can thus be regarded as a stable fixed point.

[115] F. Parisen Toldin, M. Hohenadler, F. F. Assaad, and I. F. Herbut, Phys. Rev. B **91**, 165108 (2015).

[116] This transformation proceeds as follows. Starting from Eq. (4), $m^2(\tau, L) = \tau^{-2\beta/\nu z} f_m(\tau L^{-z})$, we define $f_m(\tau L^{-z}) = (\tau L^{-z})^{2\beta/\nu z} f_{m1}(\tau L^{-z})$. Substituting back gives $m^2(\tau, L) = \tau^{-2\beta/\nu z}(\tau L^{-z})^{2\beta/\nu z} f_{m1}(\tau L^{-z}) = L^{-2\beta/\nu} f_{m1}(\tau L^{-z})$.

[117] C.-J. Yang, K. Kliemt, C. Krellner, J. Kroha, M. Fiebig, and S. Pal, Nat. Phys. **19**, 1605 (2023).

[118] Z. Zeng, Y.-K. Yu, Z.-X. Li, Z.-X. Li, and S. Yin, Nat. Commun. **16**, 6181 (2025).

[119] S. Deng, G. Ortiz, and L. Viola, Phys. Rev. B **83**, 094304 (2011).

[120] Y.-K. Yu, Z. Zeng, Y.-R. Shu, Z.-X. Li, and S. Yin, Dataset for "Nonequilibrium dynamics of dirac quantum criticality in imaginary time," 2026, 10.5281/zenodo.18488908.